Available online at www.sciencedirect.com
ScienceDirect
Journal of the European Ceramic Society 29 (2009) 1587–1594
www.elsevier.com/locate/jeurceramsoc

Influence of cassava starch content and sintering temperature on the alumina consolidation technique

F.A. Almeida [a], E.C. Botelho [b], F.C.L. Melo [c], T.M.B. Campos [c], G.P. Thim [c,*]

[a] *Department of Ceramics and Glass Engineering, CICECO, University of Aveiro, 3810-193 Aveiro, Portugal*
[b] *Department of Materials and Technology, UNESP, Guaratinguetá – SP, CEP 12516-410, Brazil*
[c] *Instituto Tecnológico de Aeronáutica, São José dos Campos – SP, CEP 12228-901, Brazil*

Received 2 April 2008; received in revised form 1 October 2008; accepted 7 October 2008
Available online 21 November 2008

Abstract

The influence of starch content and sintering temperature on the preparation of alumina bodies were studied. The process was water-based and cassava starch was used as consolidator, binder and pore former. Colloidal suspensions were prepared with three different starch concentrations and the ideal dispersant content and gel point were determined by rheological analysis. The wet samples were demolded after consolidation in silicone mold at 60 °C for 2 h. After the drying step the samples were sintered at 1200, 1400 and 1600 °C, showing open porosities between 13 and 55%, depending on the starch content on the precursor suspensions and sintering temperature. The pore structures were analyzed by SEM (scanning electron microscopy) and Hg porosimetry. Basically, the pore structures are dominated by large spherically shaped pores left by the starch particles, which are connected through small pore channels.

Keywords: Starch; Cassava; Alumina; Gel; Porosity

1. Introduction

Slurry-based process materials have been employed extensively in various types of materials generating techniques such as tape casting,[1,2] three-dimensional printing,[3,4] slip casting,[5] and dip coating.[6] Alcohols, ketones, hydrocarbons, and other organic solvents of low boiling points have been used in such process,[7] but due to their toxicity and inflammability, they are considered environmentally hazardous. Therefore, materials processing industries are replacing organic solvents for others with lower environmental impact.[8] Since the use of water-based solvents for the preparation of materials with very small thickness is already known, the use of such solvent for the preparation of thicker materials has attracted great interest.[9] The chemical, physical and mechanical properties of a green compact, such as stability, appropriate viscosity of precursor powder suspension and sufficient green strength, are determinant for a high quality thick-processed material. To achieve that result, many methods have been studied to produce homogeneous microstructured green bodies with these properties.[10] One of the most promising methods is the colloidal system, which uses a suspension obtained by dissolving a ceramic powder in an appropriate solvent. The long-term stability of a suspension is due to the repulsive forces acting among the surface charged particles.[11,12] Several powder materials have been studied to be used in water-based slurries, such as: Al_2O_3,[11–14] Y_2O_3-stabilized ZrO_2,[15–18] and cordierite.[10,19] In the past decade, water-based colloidal binders, such as: latexes,[11] cellulose ether,[8] polyvinyl alcohol (PVA),[18] albumin[20,21] and maltodextrin[22] have been investigated, aiming to produce green bodies with adequate properties. By controlling the rheological properties of the suspensions, obtained by adjusting the deflocculating content, the use of these binders was found feasible for ceramic consolidation.[23]

The preparation of porous materials with starch is a direct consolidation technique, based on starch properties of gelling in warm water, which allows its use as consolidator and pore producer.[24,25] This technique allows a good porosity control of the developed product, because the pores will be formed in the initial places of the starch grains, considering its expansion in the aqueous medium.

* Corresponding author. Fax: +55 12 39475958.
E-mail address: gilmar@ita.br (G.P. Thim).

0955-2219/$ – see front matter © 2008 Elsevier Ltd. All rights reserved.
doi:10.1016/j.jeurceramsoc.2008.10.006

Several works have been made with this technique, using different ceramics precursors such as, alumina,[21,22,24] alumina-tungsten metal–ceramic system,[9] silica,[26] alumina-silicate fiber,[27] glass-reinforced hydroxyapatite,[28] calcium carbonate,[25] yttria-stabilized zirconia,[29] mullite,[30] cordierite,[31] among others. These works demonstrated the ability to obtain porous bodies with complex shape, controllable microstructure, by using initial suspensions with different solids loading and starch types, which can be molded to several applications. Since pore structure is determined by the type of starch used, ceramic bodies with distinct porous morphology can be prepared by using starch from different sources. The most common examples are: rice,[32] potato[21,24] and corn.[9,29] Among these, potato starch exhibits the largest and most anisometric granules, while rice starch is the smallest and more isometric.[32]

The use of cassava starch as binder and pore producer is not well known as the others mentioned above. In the literature, a very recent work reports the use of this starch type to prepare silica bodies with tri-modal pore structure by using two consolidation techniques, starch and foaming.[26] The widespread employing of cassava starch can be of great interest, especially in Brazil, due to its low cost and availability, which justifies the efforts to make it a feasible raw material for ceramic parts production.

In this paper, cassava starch was used as water soluble binder for consolidating alumina bodies with different densities and porosities. Rheological studies were used to determine the experimental conditions for slurry preparation, such as: starch concentration, gelatinization conditions and dispersant content. Sintered alumina was obtained at 1200, 1400 and 1600 °C, and it was observed that the density and the porosity of the resulting material are dependent on starch concentration and sintering temperature.

2. Experimental

2.1. Raw materials and preparation of suspensions

Ceramic bodies were made with aluminum oxide (Al_2O_3) and commercial cassava starch. The characteristics of the powder precursors are as follows:

(1) *Al_2O_3 (Alcoa Chemicals, A-1000)*: density = 3.89 g/cm^3; surface area = 8.9 m^2/g; average particle size = 0.45 μm. The characteristics are from supplier's catalog;
(2) *Cassava starch (from food industry)*: density = 1.55 g/cm^3, determined by helium picnometry; bimodal particle size distribution with average values between 1.5 and 18 μm, as determined by laser diffraction method.

The colloidal suspensions were stabilized using ammonium polyacrilate dispersant (Disperlan LA) in bi-distilled water. Alumina and starch powders were sieved at # 42 mesh and added to bi-distilled water with dispersant. The suspensions were milled in a Fritsch Pulverisette equipment model 05.201, planetary type, for 15 min. The resultant mixture was agitated in an ultrasonic bath for 10 min at 40 °C. Four different colloidal suspensions were prepared and their compositions and labels are shown in Table 1.

Table 1
Chemical composition of the colloidal suspensions.

Sample (code)	Starch (vol.%)	Alumina (vol.%)	Dispersant (vol.%)	Water (vol.%)
CS-10S + 30A	10	30	0.6	59.4
CS-15S + 30A	15	30	0.6	54.4
CS-20S + 30A	20	30	0.6	49.4

2.2. Dynamic viscosity and viscoelasticity measurements

Rotational viscosity measurements were performed to determine the more adequate dispersant concentration of colloidal suspensions. The viscosimeter used was a Brookfield LV Spindle Set viscometer, at 30 rpm and shaft number 2. The temperature and time used in the gelling step of the suspensions were determined by rheological measurements, using an oscillatory rheometer from Rheometric Scientific model SR5, parallel plates, with gap of 1.00 mm, frequency of 1 rad/s and pressure of 200 Pa. The real part of the viscosity, η', is the apparent dynamic viscosity and the imaginary part of the viscosity, η'', is the measure of the elasticity. The linear viscoelastic properties, namely the complex viscosity η^* is defined as $\eta^* = \eta' - i\eta''$. The storage modulus, G′, and loss modulus, G″, are measures of the elastic and viscous properties of a system, respectively. They are the real and imaginary components of the complex modulus, G^*, where $G^* = G' + iG''$. In this work, the gel time and gel temperature were obtained tracing a tangent to the evolution of the modulus of complex viscosity ($|\eta^*|$) curve, which was determined by the following equation:

$$|\eta^*| = [(\eta')^2 + (\eta'')^2]^{1/2}.$$

2.3. Preparation of samples

The colloidal suspensions prepared with the chosen dispersant concentration were poured into a silicone mold, covered with a PVC plastic film and put into an oven for 2 h at 60 °C for the gelatinization process. After the gelling step the samples were dried for 24 h at room temperature, then they were unmolded and returned to oven, firstly at 60 °C for 12 h and then at 110 °C for 24 h. These samples, in the "green" state, were thermally analyzed using a TGA PerkinElmer-7 in synthetic air atmosphere at a flow rate of 20 mL/min and a heating rate of 10 °C/min from room temperature until 900 °C. Based on the thermogravimetric information, a thermal cycle of 5 set-point temperatures was made to control the burn out of the organic materials in a muffle furnace under air environment. Thus, calcination and pre-sintering of the samples were done at the same time, according to a determined thermal cycle with the following steps: (1) from room temperature up to 200 °C, at 3 °C/min; (2) from 200 up to 300 °C, at 1 °C/min; (3) from 300 up to 400 °C, at 1 °C/min; (4) from 400 up to 500 °C at 1 °C/min; (5) from 500 up to 1000 °C at 3 °C/min. The holding time between steps was

15 min while in the last, time was increased in 60 min. After this process, the samples were sintered at 1200, 1400 and 1600 °C, at 5 °C/min for 120 min in a NABER electric furnace. The dimensions of the sintered and green samples were compared and the linear shrinkage was determined.

2.4. Morphology evaluation of the starch gelatinization behavior

A suspension containing 5 vol.% of starch in distilled water was observed by polarized light optical microscopy (LEICA–model DMLS) coupled with a heating plate (Linkam) from room temperature until 60 °C at a heating rate of 3 °C/min. Acquisition of real-time images and analysis of the grain swelling was performed by using the "UTHSCSA Image Tool 2.0" with the routine package "Image Processing Toolkit 4.0" (Reindeer Games INC.).

2.5. Porosity characterization

Microstructural analysis of the sintered samples was conducted by using a Scanning Electronic Microscopy, LEO model 534Vpi. The water absorption, relative density and apparent porosity of these samples were determined using ASTM C20-87 normative[33] and the pore size was measured by an Hg porosimetry (Quantachrome, model Autoscan 33).

3. Results and discussion

3.1. Dispersant concentration

Fig. 1 shows the viscosity behavior of the colloidal suspensions in function of the dispersant concentration. The experimental data was fitted with an exponential decay equation, which shows that the viscosity of the colloidal suspension decreases exponentially with the increase of the dispersant concentration, reaching an approximate constant value for concentrations above 0.60% (v/v). Therefore, this dispersant amount

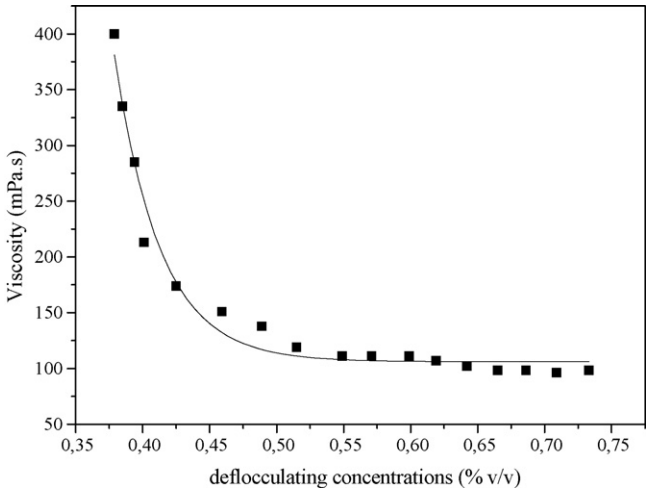

Fig. 1. Evolution of colloidal suspension viscosity as a function of dispersant concentration.

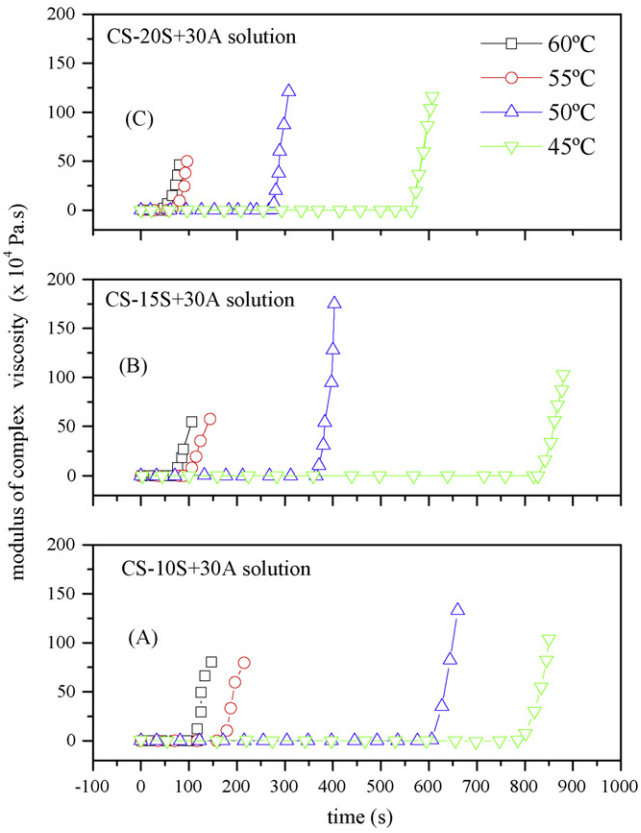

Fig. 2. Modulus of complex viscosity of CS-10S + 30A, CS-15S + 30A and CS-20S + 30A colloidal suspensions at 45, 50, 55 and 60 °C.

was considered adequate, since small variations do not change significantly the viscosity of the suspension. Subsequently, experimental tests showed that all the others colloidal suspensions prepared with this dispersant concentration were stable for long periods, allowing them to be handled in all experimental steps.

3.2. Gelatinization behavior of colloidal suspension

The gel point transition can be used to determine the experimental conditions for a colloidal suspension to undergo the sol–gel transition. In this work the gel point was determined by the analyses of isothermal curves of complex viscosity. Fig. 2 shows the evolution of the complex viscosity with time of the colloidal suspensions CS-10S + 30A (Fig. 2a), CS-15S + 30A (Fig. 2b) and CS-20S + 30A (Fig. 2c), at four isothermal conditions, 45, 50, 55 and 60 °C. The sol to gel transition is clearly shown by the abrupt change in the viscosity behavior. Fig. 2 also indicates that the conditions for the sol to gel transition are determined by the starch concentration, temperature and heating period. Generally, for a specific temperature, the gelatinization time is inversely proportional to the starch concentration, and for a given starch concentration in the colloidal suspension, the gelatinization time is also inversely proportional to the heating temperature.

Therefore, once the heating temperature is chosen for each of the three different colloidal suspensions, the minimum period

Table 2
Gelatinization time for several isothermals.

Temperature (°C) Isothermal	Gelation time (s) CS-10S + 30A	Gelation time (s) CS-15S + 30A	Gelation time (s) CS-20S + 30A
45	821	789	559
50	604	362	279
55	164	107	88
60	100	69	62

to obtain the gels is determined from its corresponding curve in Fig. 2. Table 2 shows the minimum gelatinization time for each isothermal and colloidal suspension. It can be seen that the viscosity behavior changes abruptly for all isothermal conditions, but faster for temperatures above 55 °C. It is reported that at temperatures near 60 °C, a breakage of the hydrogen bonding from amylose and amylopectin molecules from starch occurs, allowing the surrounding water to be absorbed by the chains at a high rate.[34] The consequent swelling of the starch grains induces the gel formation, thus increasing the suspension viscosity.

This rheological behavior can be better visualized in Fig. 3a–d, where the polarized light optical micrographs (taken at 45, 50, 55 and 60 °C, respectively) show the changing of the characteristic starch grain birefringence with temperatures above 55 °C. The sample heated at 45 and 50 °C (Fig. 3a and b, respectively) show that the particles grain size does not vary at these temperatures (in the absence of holding times) and have a nearly spherical morphology. Though, a noticeable change can be observed when Fig. 3b and c are compared. This change is related to the appearance of some particles approximately two times larger than the original ones, thus providing a clear indication that the gelatinization process is starting. Also, it is evident that the starch globules do not grow at the same rate, since a considerable faster growth of particles of larger size is visible. This statistical starch swelling behavior was also noticed by Týnová and co-workers.[35] They performed viscometric and real-time microscopic studies of potato starch in aqueous suspension heated up to 56 °C. The particles observed at 60 °C (Fig. 3d) are bigger than those at 55 °C (Fig. 3c), but the noticeable observation is the quantity of swelled particles, hence indicating that at this temperature the gelatinization rate is higher than at 55 °C. The time range in which the gel transition occurs for all suspensions at 60 °C is between 62 and 100 s, for the highest starch content suspension (CS-20S + 30A, Fig. 2c) and the lowest one (CS-10S + 30A, Fig. 2a), respectively (Table 2). Surprisingly, and in the same way, an increment of the viscosity also occurs for lower temperatures (45 and 50 °C), between 279 s for the highest starch content and 821 for the lowest one. Although the micrographs on Fig. 3a and b do not show any swelling effect at these temperatures (45 and 50 °C, respectively), at no holding time condition, such increment on the viscosity behavior can be a consequence of mechanical/thermal activation during milling, and also a result of the dynamic friction caused by the oscillatory movement at constant pressure of the parallel plates rheometer.

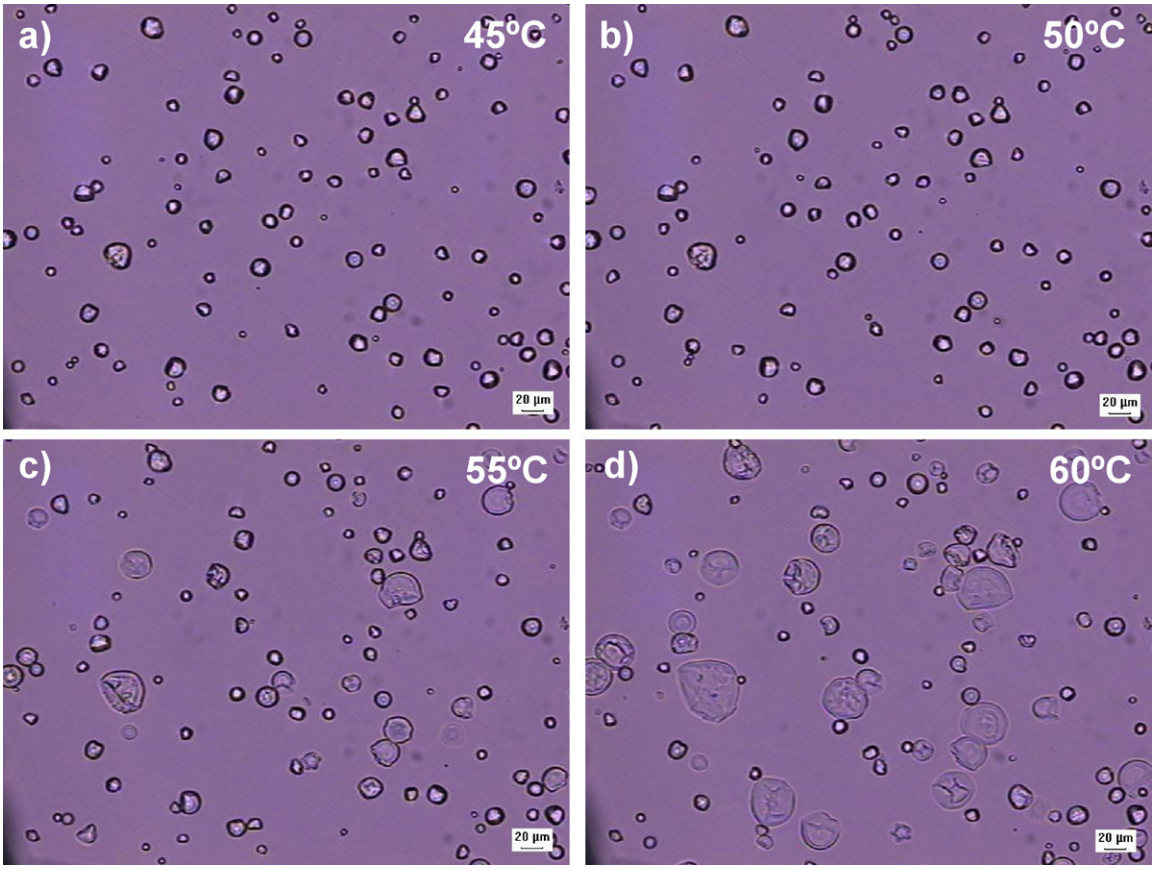

Fig. 3. Micrographs of starch grains in water at following temperatures: (a) 45; (b) 50; (c) 55 and (d) 60 °C.

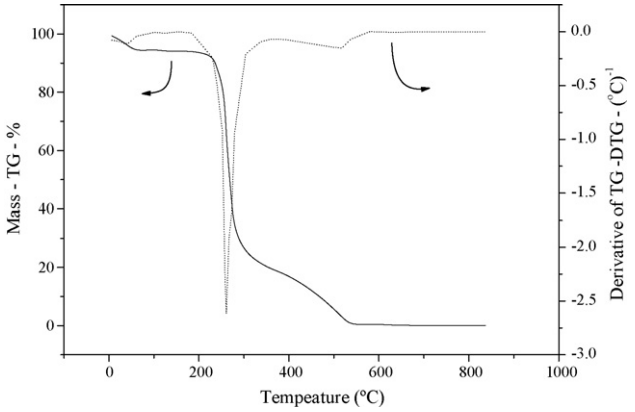

Fig. 4. TGA and DTG curves for cassava starch in synthetic air atmosphere.

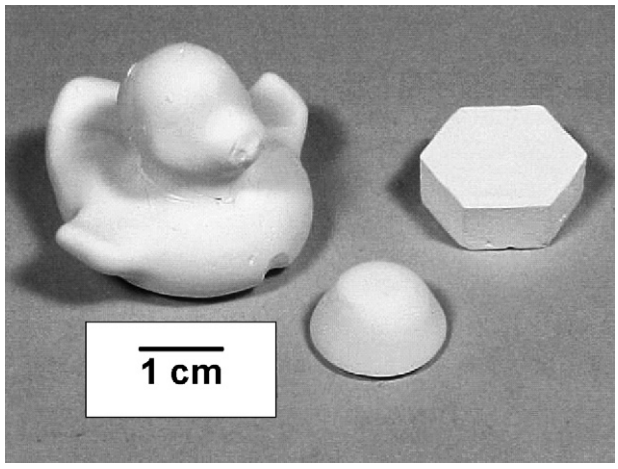

Fig. 5. Some examples of sintered alumina bodies obtained from starch consolidation technique.

Therefore, it is supposed here that these events may activate the glucose chains breakage, allowing the swelling of the grains at such low temperatures. However, systematic studies need to be done in order to better clarify the individual contributions of each event to the earlier swelling of the grains. Nevertheless, this earlier gelatinization can be feasible, since tapioca starch (that is derived from cassava root) has the lowest temperature of gelatinization in excess of water (49 °C) among potato, wheat, corn and rice starches.[32]

According to this behavior, when the starch grains swell, the ceramic particles around them becomes highly compacted by water drainage from the slurry, forcing the particles to stick together and, as a result, consolidating the suspension into a rigid body.[24] A tridimensional network including the volume occupied by the starch, water and immobilized alumina particles are thus formed[36,37] The time spent in the suspension gelatinization process (consolidation step) should be minimized to avoid particles segregation and, consequently, the lack of homogeneity of the green bodies. For the consolidation of green bodies, the same time and temperature for the gelation of the three colloidal suspensions were used. The shorter periods of gelation time were obtained at 60 °C; among these, CS-10S + 30A colloidal suspension showed the longest gelation time. Therefore, the gelation conditions for all colloidal suspensions were based on the rheological measurements performed for the CS-10S + 30A colloidal suspension at 60 °C. In accordance with Table 2, this condition is: 60 °C and 100 s.

3.3. Thermal decomposition of cassava starch

Thermogravimetric analysis (TGA) was performed on green samples in order to analyze the breakdown that amylose and amylopectin undergo when subjected to high temperatures. Thermogravimetric (TG) and derivative thermogravimetric curves (DTG) are shown in Fig. 4. They show that starch starts degrading at about 250 °C and continues to loose weight up to 500 °C. It can be observed that the weight loss occurs by a two step degradation process. The first one begins at around 190 °C and finishes at 355 °C, which corresponds to the complete breakdown of starch; the second one starts at around 360 °C and ends at 580 °C, and it is attributed to the oxidation of partially decomposed starch.[25] The first one begins at around 190 °C and finishes at 355 °C and the second one starts at around 360 °C and ends at 580 °C. The degradation of corn starch was investigated by Aggarwal[38] under air and nitrogen atmospheres. He observed that the degradation process occurs by one step under nitrogen atmosphere and by two steps under air atmosphere. For the two types of experiments the first step start at approximately 250 °C and the second one starts at around 360 °C. As corn and cassava starches are very similar, the Aggarwal conclusions could be extended to the thermal studies of cassava starch. Therefore, the first thermal event observed during the cassava starch decomposition could be attributed to the starch complete breakdown, and the second one could be related to the oxidation of partially decomposed starch.

3.4. Sintered samples properties

Sintering was performed without significant anisotropic shrinkage, which indicates the good homogeneity of the materials. Fig. 5 shows some examples of various sintered components, illustrating the high versatility in shape and size that can be obtained by using this technique.

Table 3 shows the results (average values of four samples of each batch) of the relative density (ρ), linear shrinkage (R_L), water absorption (A_w) and apparent porosity (P), determined for the sintered bodies at different starch concentration and sintering temperature. The relative density values of the sintered bodies are calculated from theoretical density of α-alumina (= 3.98 g cm^{-3}). These values are dependent on sintering temperature and starch contents of the original colloidal suspensions. In general, the relative density increases with decreasing starch content, at the same sintering temperatures. For instance, the relative densities of the bodies sintered at 1200 °C are in the range of (0.42 ± 0.03) to (0.54 ± 0.01) of the theoretical density of alumina and the porosities values are from (43.5 ± 0.7) to (55.5 ± 0.3)%. The water absorption is proportional to porosity, varying from (20.3 ± 0.3)% to (33.1 ± 0.3)%. For samples with the same starch content, the relative density

Table 3
Relative density (ρ), apparent porosity (P), water absorption (A_w) and linear shrinkage (R_L) for the CS-10S + 30A, CS-20S + 30A and CS-30S + 30A samples sintered at 1200, 1400 and 1600 °C.

Sample/sintering temperature (°C)	ρ	P (%)	A_w (%)	R_L (%)
CS-10S + 30A/1200	0.54 ± 0.01	43.5 ± 0.7	20.3 ± 0.3	15.2 ± 0.4
CS-10S + 30A/1400	0.60 ± 0.04	32.9 ± 0.7	13.7 ± 0.5	21.6 ± 0.7
CS-10S + 30A/1600	0.74 ± 0.01	13.1 ± 0.9	4.4 ± 0.2	24.9 ± 0.6
CS-15S + 30A/1200	0.48 ± 0.05	49.6 ± 0.9	26.0 ± 0.4	17.0 ± 0.8
CS-15S + 30A/1400	0.59 ± 0.01	36.4 ± 0.9	15.6 ± 0.7	23.9 ± 0.5
CS-15S + 30A/1600	0.69 ± 0.02	25.7 ± 0.6	9.4 ± 0.3	27.6 ± 0.7
CS-20S + 30A/1200	0.42 ± 0.03	55.5 ± 0.3	33.1 ± 0.3	19.6 ± 0.6
CS-20S + 30A/1400	0.55 ± 0.03	43.4 ± 0.7	19.9 ± 0.5	26.1 ± 0.7
CS-20S + 30A/1600	0.61 ± 0.01	38.0 ± 0.7	15.7 ± 0.3	29.6 ± 0.3

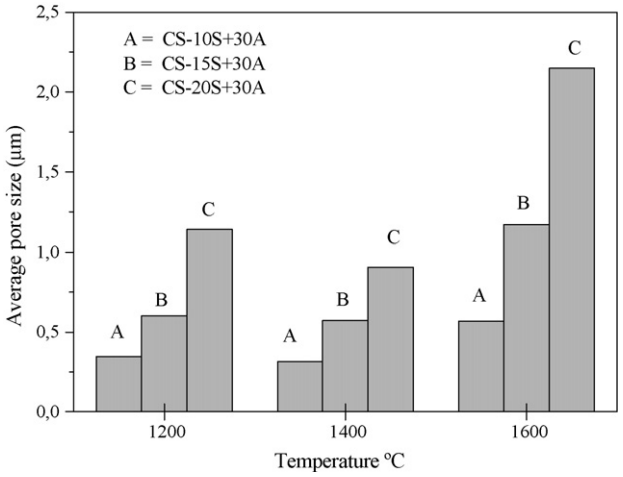

Fig. 6. Average pore size of the materials obtained from suspensions with different starch contents and sintered at 1200, 1400 and 1600 °C.

increases with the increasing of temperature, but the porosity and water absorption decrease. As for relative density, the linear shrinkage depends on starch content and sintering temperature. However, the linear shrinkage values increase with the increasing of the starch contents and also with sintering temperatures. Therefore, the lowest linear shrinkage (15.2 ± 0.4)% was observed for bodies prepared from CS-10S + 30A suspension and fired at 1200 °C, while the highest one (29.6 ± 0.3)% was observed from the CS-20S + 30A suspension sintered at 1600 °C. Because of the correlation of these structural properties, it is possible to produce bodies with similar relative density using a correct combination of starch contents and sintering temperatures. For example, bodies with relative density near to 0.60 can be obtained using: CS-10S + 30A suspension and firing at 1400 °C, CS-15S + 30A suspension and firing at 1400 °C and CS-20S suspension and firing at 1600 °C.

3.5. Microstructure and Hg porosimetry of the sintered samples

The microstructure of the sintered samples was studied in terms of porosity by two complementary techniques: Hg porosimetry and SEM investigations. Hg porosimetry was used to measure the smaller pores, which correspond to the connecting contact areas between larger pores. On the other hand, SEM investigations displayed the overall pore structure, which is dominated by the large pores left by starch particles. Fig. 6 shows the average pore size, by Hg porosimetry technique, of sintered materials obtained from CS-10S + 30A, CS-15S + 30A and CS-20S + 30 colloidal suspensions and sintered at 1200, 1400 and 1600 °C. It displays how the average pore size is dependent on the starch contents and sintering temperatures. By increasing the starch content, there is an expected increase in the pore size and also in the number and degree of contacts between

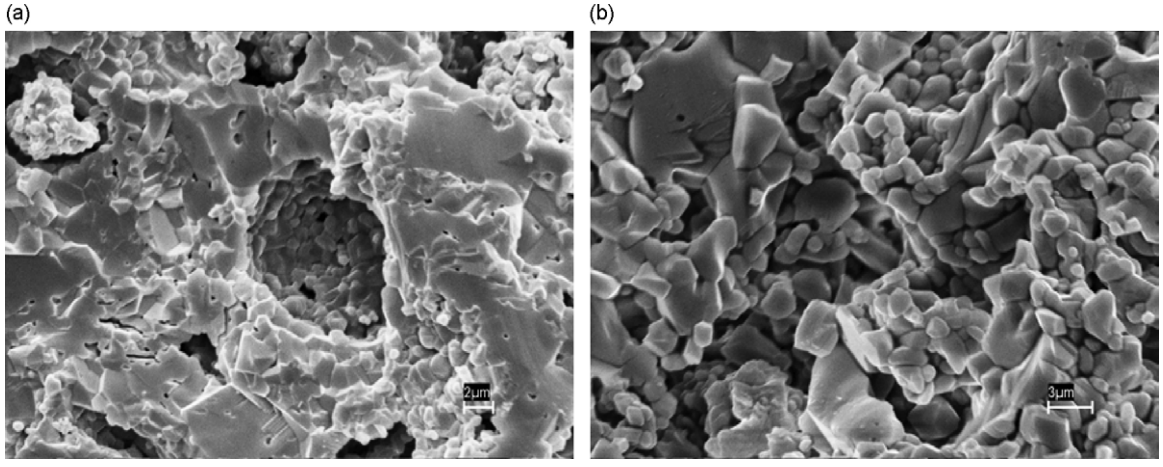

Fig. 7. SEM images of fractured surfaces of the alumina materials sintered at 1600 °C, obtained from (a) CS-10S + 30A and (b) CS-20S + 30A colloidal suspensions.

the starch particles, resulting in a larger average pore size. It also becomes larger with the sintering temperature. One possible explanation is, as the sintering temperature increases, the alumina interparticle necks are increased leading to more effective pore shrinkage. Therefore, by rising the temperature, it is possible to eliminate the smaller pores of the alumina matrix (the interconnecting pores). Fig. 7 shows a representative SEM images of the microstructure of two sintered alumina materials, obtained from CS-10S + 30A and CS-20S + 30A suspensions. The large, spherically shaped pores correspond well to the shape and size of the original starch particles.

4. Conclusions

A water-based method was presented to prepare alumina green compact using cassava starch as a binder. The method proved to be versatile, enabling to prepare ceramic bodies with complex geometry, several densities and porosities. The process is based on body conformation from colloidal suspension which changes to gel in an oven at 60 °C. The dispersant contents and gel point were determined by rheological analysis. Sintered samples were prepared at 1200, 1400 and 1600 °C; microstrutural studies showed that sample densities and porosities were a function of starch contents and sintering temperature. The sintered samples presented relative density in the range of 0.4–0.75 and open porosity in the range of 13–55%, depending on the starch content of the precursor suspensions and sintering temperature.

Acknowledgements

Authors gratefully acknowledge CAPES and CNPq for financial support. F.A. Almeida also acknowledges FCT for the grant SFRH/BPD/26787/2006.

References

1. Iverson, B., Kim, H. J., Slamovich, E. and Bowman, K., Texture evolution in tape cast lead metaniobate. *J. Eur. Ceram. Soc.*, 2008, **28**(4), 863–869.
2. Yoon, D. H. and Lee, B. I., Effects on aqueous barium titanate tape properties of passivation of barium ion leaching by using dispersants. *J. Eur. Ceram. Soc.*, 2004, **24**(15–16), 3747–3752.
3. Sachs, E. and Cima, M., Three dimensional printing. Rapid tooling and prototypes directly from a CAD model. *J. Eng. Ind.*, 1992, **114**, 481–488.
4. Sachs, E., Cima, M. and Bredt, J., Three-dimensional printing of ceramic shells and cores for metal casting. *Am. Soc. Mech. Eng.*, 1991, **50**, 61–72.
5. Azar, M., Palmero, P., Lombardi, M., Garnier, V., Montanaro, L., Fantozzi, G. *et al.*, Effect of initial particle packing on the sintering of nanostructured transition alumina. *J. Eur. Ceram. Soc.*, 2008, **28**(6), 1121–1128.
6. Aegerter, M. A. and Mennig, M., *Sol–Gel Technologies for Glass Producers and Users*. Kluwer Academic Publishers, Norwell, MA, 2004, pp. 37–48.
7. Hotza, D. and Greil, D. P., Review: aqueous tape casting of ceramic powders. *Mater. Sci. Eng. A*, 1995, **202**, 206–217.
8. Kristoffersson, A., Roncari, E. and Galassi, C., Tape casting of alumina in water with an acrylic latex binder. *J. Eur. Ceram. Soc.*, 1998, **18**, 2123–2131.
9. LeBeau, J. M. and Boonyongmaneerat, Y., Comparison study of aqueous binder systems for slurry-based processing. *Mater. Sci. Eng. A*, 2007, **458**, 17–24.
10. Bitterlich, B., Lutz, C. and Roosen, A., Rheological characterization of water-based slurries for the tape casting process. *Ceram. Int.*, 2002, **28**(6), 675–683.
11. Napper, D. H., *Polymeric Stabilization of Colloidal Dispersions*. Academic Press, New York, 1983.
12. Horn, R. G., Surface forces and their action in ceramic materials. *J. Am. Ceram. Soc.*, 1990, **73**(5), 1117–1135.
13. Doreau, F., Tarì, G., Pagnoux, C., Chartier, T. and Ferreira, J. M. F., Processing of aqueous tape-casting of alumina with acrylic emulsion binders. *J. Eur. Ceram. Soc.*, 1998, **18**(4), 311–321.
14. Doreau, F., Tarì, G., Guedes, M., Chartier, T., Pagnoux, T. C. and Ferreira, J. M. F., Mechanical and lamination properties of alumina green tapes obtained by aqueous tape casting. *J. Eur. Ceram. Soc.*, 1999, **19**(16), 2867–2873.
15. Pagnoux, C., Chartier, T., Granja, M. F., Ferreira, J. M. F. and Baumard, J. F., Aqueous suspensions for tape-casting based on acrylic binders. *J. Eur. Ceram. Soc.*, 1998, **18**, 241–247.
16. Renger, C., Kuschel, P., Kristoffersson, A., Clauss, B., Oppermann, W. and Sigmund, W., Rheology studies on highly filled nano-zirconia suspensions. *J. Eur. Ceram. Soc.*, 2007, **27**(6), 2361–2367.
17. Lan, W. and Xiao, P., Drying stress of yttria-stabilized-zirconia slurry on a metal substrate. *J. Eur. Ceram. Soc.*, 2007, **27**(10), 3117–3125.
18. Albano, M. P. and Garrido, L. B., Aqueous tape casting of yttria stabilized zirconia. *Mater. Sci. Eng. A*, 2006, **420**, 171–178.
19. Costa Oliveira, F. A., Dias, S., Fátima Vaz, M. and Cruz Fernandes, J., Behaviour of open-cell cordierite foams under compression. *J. Eur. Ceram. Soc.*, 2006, **26**(1–2), 179–186.
20. Lyckfeldt, O., Brandt, J. and Lesca, S., Protein forming: a novel shaping technique for ceramics. *J. Eur. Ceram. Soc.*, 2000, **20**, 2551–2559.
21. Bhattacharjee, S., Besra, L. and Singh, B., Effect of additives on the microstructure of porous alumina. *J. Eur. Ceram. Soc.*, 2007, **27**, 47–52.
22. Kim, J. C., Auh, K. O. and Schiling, C. H., Effects of polyssacharides on the rheology of alumina slurries. *J. Eur. Ceram. Soc.*, 2000, **20**, 259–266.
23. Mei, S., Yang, J., Xu, X., Quaresma, S., Agathopoulos, S. and Ferreira, J. M. F., Aqueous tape casting processing of low dielectric constant cordierite-based glass-ceramics—selection of binder. *J. Eur. Ceram. Soc.*, 2006, **26**, 67–71.
24. Lyckfeldt, O. and Ferreira, J. M. F., Processing of porous ceramics by 'Starch Consolidation'. *J. Eur. Ceram. Soc.*, 1998, **18**, 131–140.
25. Lemos, A. F. and Ferreira, J. M. F., Porous bioactive calcium carbonate implants processed by starch consolidation. *Mater. Sci. Eng. C*, 2000, **11**, 35–40.
26. Mao, X., Wang, S. and Shimai, S., Porous ceramics with tri-modal pores prepared by foaming and starch consolidation. *Ceram. Int.*, 2008, **34**, 107–112.
27. Lidén, E., Karlsson, S. and Tokarz, B., Silica sols as refractory fibre binders. *J. Eur. Ceram. Soc.*, 2001, **21**, 795–808.
28. Prado da Silva, M. H., Lemos, A. F., Gibson, I. R., Ferreira, J. M. F. and Santos, J. D., Porous glass reinforced hydroxyapatite materials produced with different organic additives. *J. Non-Cryst. Solids*, 2002, **304**, 286–292.
29. Sanson, A., Pinasco, P. and Roncari, E., Influence of pore formers on slurry composition and microstructure of tape cast supporting anodes for SOFCs. *J. Eur. Ceram. Soc.*, 2008, **28**(6), 1221–1226.
30. Barea, R., Osendi, M. I., Ferreira, J. M. F. and Miranzo, P., Thermal conductivity of higly porous mullite material. *Acta Mater.*, 2005, **53**, 3313–3318.
31. Alves, H. M., Tarì, G., Fonseca, A. T. and Ferreira, J. M. F., Processing of porous cordierite bodies by starch consolidation. *Mater. Res. Bull.*, 1998, **33**, 1439–1448.
32. Gregorová, E., Pabst, W. and Bohacenko, I., Characterization of different starch types for their application in ceramic processing. *J. Eur. Ceram. Soc.*, 2006, **26**, 1301–1309.
33. Annual American Standard Test Methods *C20-87*. Standard test methods for apparent porosity, water absorption, apparent specific gravity, and bulk density of burned refractory brick and shapes by boiling water. Philadelphia, 1988. pp. 5–7.
34. Bobbio, F. O. and Bobbio, P., *Introdução à Química de Alimentos* (*5th ed.*). Livraria Varela, São Paulo, 1989, p. 49.

35. Týnová, E., Pabst, W. and Mikac, J., Starch swelling and its role in modern ceramic shaping technology. *Macromol. Symp.*, 2003, **203**, 295–300.
36. Segrè, P. N., Prasard, V., Schofield, A. B. and Weitz, D. A., Glasslike kinetic arrest at the colloidal-gelation transition. *Phys. Rev. Lett.*, 2001, **86**, 6042–6045.
37. Berli, C. L. A., Rheology and phase behavior of aggregating emulsions related to droplet–droplet interactions. *Braz. J. Chem. Eng.*, 2007, **24**(2), 203–210.
38. Aggarwal, P., Dollimore, D. and Heon, K., Comparative thermal analysis study of two biopolymers, starch and cellulose. *J. Thermal Anal.*, 1997, **50**, 7–17.